Minimal basilar membrane motion in low-frequency hearing

Rebecca L. Warren[a,1], Sripriya Ramamoorthy[b,1], Nikola Ciganović[c], Yuan Zhang[d], Teresa M. Wilson[d], Tracy Petrie[e], Ruikang K. Wang[f,g], Steven L. Jacques[e,h], Tobias Reichenbach[c], Alfred L. Nuttall[d,2], and Anders Fridberger[a,d,2]

[a]Department of Clinical and Experimental Medicine, Linköping University, SE-58183 Linköping, Sweden; [b]Department of Mechanical Engineering, Indian Institute of Technology Bombay, Mumbai, Maharashtra 400076, India; [c]Department of Bioengineering, Imperial College, London SW7 2AZ, United Kingdom; [d]Oregon Hearing Research Center, Department of Otolaryngology, Oregon Health & Science University, Portland, OR 97239-3098; [e]Department of Biomedical Engineering, Oregon Health & Science University, Portland, OR 97239; [f]Department of Bioengineering, University of Washington, Seattle, WA 98195-5061; [g]Department of Ophthalmology, University of Washington, Seattle, WA 98195-5061; and [h]Department of Dermatology, Oregon Health & Science University, Portland, OR 97239;

Edited by Christopher A. Shera, Massachusetts Eye and Ear Infirmary, Boston, MA, and accepted by Editorial Board Member Charles F. Stevens June 11, 2016 (received for review April 23, 2016)

Low-frequency hearing is critically important for speech and music perception, but no mechanical measurements have previously been available from inner ears with intact low-frequency parts. These regions of the cochlea may function in ways different from the extensively studied high-frequency regions, where the sensory outer hair cells produce force that greatly increases the sound-evoked vibrations of the basilar membrane. We used laser interferometry in vitro and optical coherence tomography in vivo to study the low-frequency part of the guinea pig cochlea, and found that sound stimulation caused motion of a minimal portion of the basilar membrane. Outside the region of peak movement, an exponential decline in motion amplitude occurred across the basilar membrane. The moving region had different dependence on stimulus frequency than the vibrations measured near the mechanosensitive stereocilia. This behavior differs substantially from the behavior found in the extensively studied high-frequency regions of the cochlea.

hearing | basilar membrane | optical coherence tomography | hair cells

Sound causes traveling waves to propagate within the fluids of the inner ear and along the basilar membrane, from the base of the cochlea toward its apex (1–4). These waves move the sensory hair cells, deflect their stereocilia, and lead to receptor potential generation and modulation of spike rates in the auditory nerve. Because of systematic variations in basilar membrane properties, high-frequency sound stimulates sensory cells near the base of the cochlear spiral, whereas the low sound frequencies that are most important for speech and music perception cause maximal stimulation of hair cells near the apex of the spiral.

Importantly, the sensory outer hair cells of the organ of Corti are mechanically active: Their soma changes length upon electrical stimulation (5, 6), and their hair bundles can provide force (7–9). Recent theoretical and experimental work showed that forces produced by the outer hair cells feed back into the sound-evoked motion of the basilar membrane and amplify the fluid motion associated with the traveling wave (10–12). The amplitude of the traveling wave therefore grows successively as it moves forward, causing a 1,000-fold increase of sound-evoked basilar membrane motion at the place of maximum vibration (13)—at least in the high-frequency regions of the cochlea. The functionally important low-frequency parts of the inner ear appear to behave in a different manner, however.

Specifically, a recent mathematical model suggested a "ratchet" behavior, where the sensory outer hair cells amplify sound-evoked motion close to stereocilia, but not at the basilar membrane (14). If the theory has merit, basilar membrane movements are expected to be quite small, to be uninfluenced by hair-cell force generation, and to peak at a frequency that is unrelated to the frequency at which the hair bundles vibrate with their largest amplitude, a behavior distinct from the behavior found in the high-frequency regions.

Some experimental reports do indeed suggest that basilar membrane movements are smaller than vibrations measured near the hair bundles (15–18), but other studies had opposite results (19–21). In several of these measurements, there are doubts about the regions being measured from as well as the health of the preparations. However, optical coherence tomography allows sound-evoked vibration to be measured without opening the bone surrounding the hearing organ (22, 23), which makes it possible to study the organ of Corti in a state more closely resembling the natural one.

Here, we used optical coherence tomography in vivo combined with laser interferometry in vitro to investigate the sound-evoked motions and frequency selectivity at the basilar membrane and near the hair bundles so as to clarify the mechanism for detecting the low-frequency sounds on which we rely for speech and music perception.

Results

Initial experiments were performed on isolated preparations of the guinea pig temporal bone (24, 25). Sound stimulation occurred through the intact middle ear ossicles, and the resulting cellular movements of the organ of Corti (Fig. 1*A*) were measured with a laser interferometer integrated with a laser scanning confocal microscope (26).

Significance

To perceive speech, the brain relies on inputs from sensory cells located near the top of the spiral-shaped cochlea. This low-frequency region of the inner ear is anatomically difficult to access, and it has not previously been possible to study its mechanical response to sound in intact preparations. Here, we used optical coherence tomography to image sound-evoked vibration inside the intact cochlea. We show that low-frequency sound moves a small portion of the basilar membrane, and that the motion declines in an exponential manner across the basilar membrane. Hence, the response of the hearing organ to speech-frequency sounds is different from the one evident in high-frequency cochlear regions.

Author contributions: S.R., T.R., A.L.N., and A.F. designed research; T.R. conceived the original idea; R.L.W., S.R., N.C., Y.Z., T.M.W., and A.F. performed research; T.P., R.K.W., and S.L.J. contributed new reagents/analytic tools; R.L.W., S.R., N.C., and A.F. analyzed data; and R.L.W., N.C., T.R., and A.F. wrote the paper.

The authors declare no conflict of interest.

This article is a PNAS Direct Submission. C.A.S. is a guest editor invited by the Editorial Board.

Freely available online through the PNAS open access option.

[1]R.L.W. and S.R. contributed equally to this work.

[2]To whom correspondence may be addressed. Email: nuttall@ohsu.edu or anders.fridberger@liu.se.

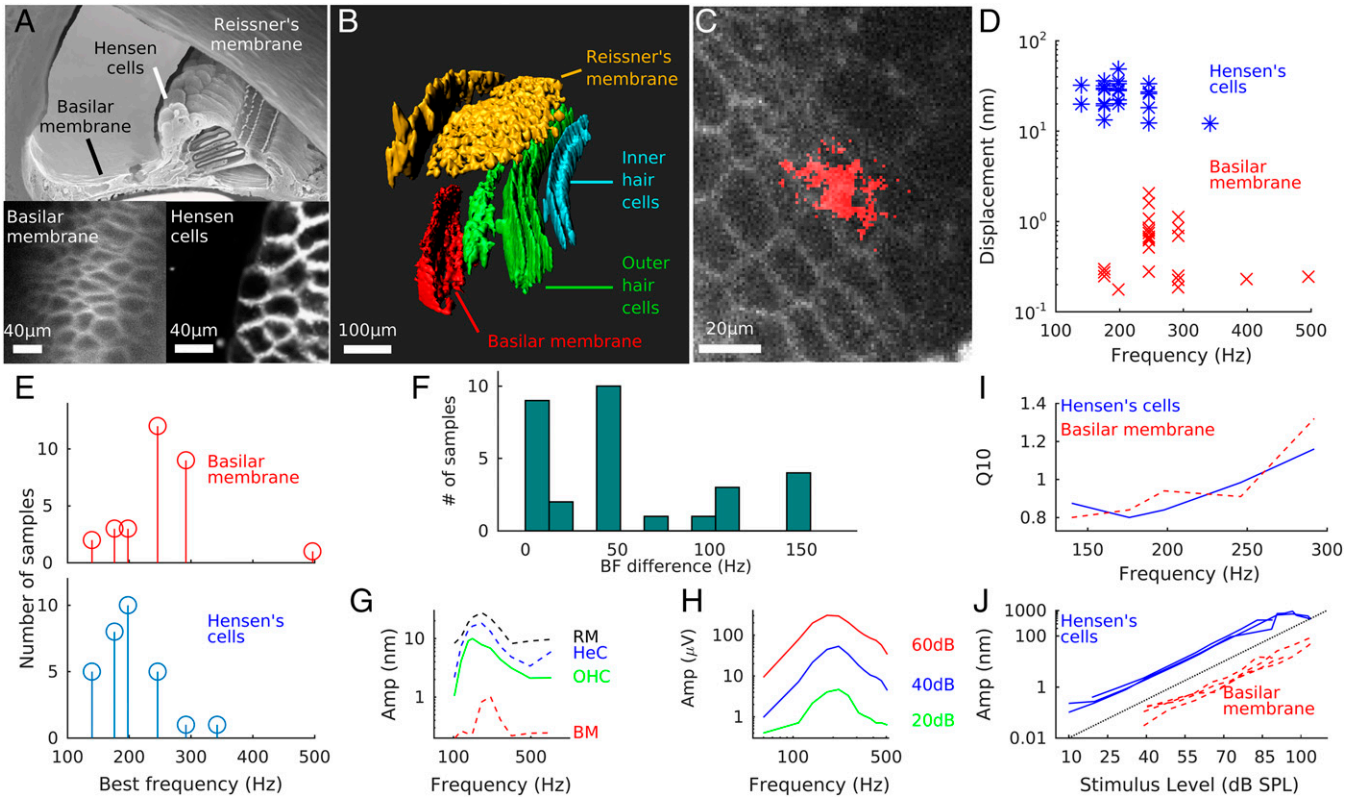

Fig. 1. Sound-evoked movements of the lateral segment of the basilar membrane are small in isolated preparations. (*A*) Schematic drawing of the organ of Corti indicating the approximate measurement locations on the basilar membrane and the Hensen cells. (*Lower Left*) Basilar membrane is identified with confocal microscopy, revealing a honeycomb-like pattern of cells. (*Lower Right*) Hensen cells are found near the stereocilia of the outer hair cells. (*B*) Three-dimensional reconstructions obtained from confocal image stacks with 4-µm section spacing were used for determining the spatial relations between measurement sites. (*C*) Absolute location of the measurement spot was determined by confocal imaging of the focused measurement beam (red dots, here focused on the basilar membrane). (*D*) Peak basilar membrane displacement is smaller than peak Hensen cell vibration. The stimulus level is 59 dB SPL. Note that all sound pressures given in this figure were corrected for attenuation caused by immersion of the preparation in tissue culture medium (*Methods*). (*E*) At 59 dB SPL, basilar membrane vibrations peak at higher frequencies in most preparations. (*F*) Frequency difference ranges from 0 to 150 Hz. In no case was the basilar membrane tuned to a lower frequency than the Hensen cells. BF, best frequency. (*G* and *H*) Mechanical tuning curves are of similar shape as the tuning of the cochlear microphonic potentials. Sound pressure in *G* was 59 dB SPL. Amp, amplitude. (*I*) Sharpness of tuning does not differ between the basilar membrane and the Hensen cells. (*J*) Hensen cells show compressive nonlinearity at levels >85 dB SPL.

Previous studies on this in vitro preparation showed that the opening in the bone, which is necessary to gain optical access to the sensory cells, leads to frequency tuning curves that are sharper than those frequency tuning curves likely to be observed in vivo (27). This effect occurs because the opening creates a pressure release pathway, which reduces the effective stimulus level at frequencies below 300 Hz (the opening is expected to influence current-evoked motion relatively less than stapes-evoked motion). To remove concerns about the influence of the opening as well as other potential artifacts (16), we used optical coherence tomography to measure sound-evoked motion in vivo, without opening the cochlear bone.

In the in vitro experiments, mechanical responses were measured at two different sites. The main one was on the basilar membrane (Fig. 1*A*, *Lower Left*), and for comparison and as a control, data were collected from the Hensen cells (Fig. 1*A*, *Lower Right*) located close to the mechanosensitive stereocilia of the outer hair cells. Spatial relations were ascertained from 3D reconstructions of confocal image stacks (Fig. 1*B*), and the absolute measurement position was confirmed by imaging the interferometer's laser spot (Fig. 1*C*).

The Lateral Segment of the Basilar Membrane Shows Minimal Sound-Evoked Motion, Different Frequency Tuning, and Smaller Dynamic Range than the Hensen Cells. We first investigated sound-evoked responses in vitro and found that basilar membrane vibrations were small, even at the stimulus frequency that evoked a maximal response [0.6 ± 0.1 nm, mean ± SEM; 59 dB of sound pressure level (SPL); $n = 30$]. In contrast, at the same SPL, the Hensen cell magnitude at the best frequency was 27 ± 2 nm, a 33-dB difference (Fig. 1*D*; $P = 1.8 \times 10^{-9}$ by the sign test). Because of anatomical constraints, all basilar membrane vibration measurements originated from a region between 10 and 40 µm from its attachment to the lateral wall of the cochlea [the distance between the attachment point and the organ of Corti is 70–75 µm (28); see Fig. 4].

To determine whether the frequency tuning of this lateral segment of the basilar membrane differs from the Hensen cells, we used a 10-tone stimulus with components between 105 and 605 Hz. The stimulus frequency evoking a maximal response at the basilar membrane varied from 140 to 496 Hz, with an average of 253 ± 12 Hz (Fig. 1*E*), whereas the average best frequency at the Hensen cells was 199 ± 9 Hz (range: 140–350 Hz). The majority of preparations ($n = 22$) showed a higher best frequency at the basilar membrane (mean difference of 54 ± 10 Hz, ~0.35 octaves; Fig. 1*F*). Eight preparations showed no difference; however, the frequency spacing of our stimulus meant that we were unable to detect differences <20 Hz. The frequency difference was statistically significant ($P = 9.5 \times 10^{-7}$ by the sign test).

Sound-evoked vibration amplitudes depend strongly on the distance from the base of the cochlea. Hence, the above findings could result from a lack of geometric registration between the two

measurement sites. To exclude this possibility, the distance between the two measured points was determined from 3D reconstructions (e.g., Fig. 1*B*). The longitudinal distance was found to be 20 ± 7 μm (range: 2–90 μm), which is too small to explain the observed frequency difference (the vertical distance between the Hensen cells and the basilar membrane varied from 120 to 180 μm).

To ensure that these basilar membrane measurements accurately reflected its motion, we had to confirm that the signal-to-noise ratio was adequate. Both the outer hair cells and Reissner's membrane, which have reflectivity close to the reflectivity of the basilar membrane, showed sound-evoked motion similar to the Hensen cells (Fig. 1*G*), as described previously (17). The large-magnitude difference between the basilar membrane and Reissner's membrane is partly related to differences in the location of the measurement (Reissner's membrane data were acquired close to its center, whereas basilar membrane measurements came from a region 10–40 μm medial to its attachment). As an additional control, we measured from the bony edge of the cochlea and found bone vibrations during sound stimulation to be an order of magnitude smaller than the basilar membrane's.

Maintaining the viability of the preparations was important. To ascertain the health of each sample, the cochlear microphonic potentials were measured (Fig. 1*H*). These alternating extracellular field potentials are generated by mechanically sensitive ion channels responding to sound stimulation, which, in our case, were continuous tones at frequencies between 60 and 510 Hz. All preparations included in this report had cochlear microphonic potential amplitude larger than 100 μV at 59 dB SPL, and the best frequency shifted downward as the sound level increased, indicative of a physiologically good preparation. Over this range of stimulus levels, little nonlinearity was present, in contrast to cochlear microphonic data acquired from the base of the cochlea in vivo.

The quality factor, Q_{10}, of the sound-evoked tuning curves was extracted for each location. The Q_{10} is determined by the frequency bandwidth 10 dB below the peak of the tuning curve, and is used as a measure of the sharpness of tuning (Fig. 1*I*). There were no significant differences, but higher Q_{10}s were observed in preparations with a high best frequency, consistent with measurements from auditory nerve fibers (29).

At the base of the cochlea, basilar membrane responses do not grow in proportion to an increase in stimulus level, but exhibit a compressive nonlinearity that yields a large dynamic range (30). To determine whether such is the case at the apex, vibration magnitudes were characterized at a variety of stimulus levels (Fig. 1*J*). A linear relation was evident through most of the range, but Hensen cell vibration showed strong saturation at levels higher than 85 dB SPL. Such saturation was not seen at the basilar membrane. It was possible to measure vibration at the Hensen cells at levels down to 20 dB SPL, but basilar membrane movement fell to the noise floor at around 40 dB SPL.

Electrical Stimulation Does Not Move the Lateral Basilar Membrane Segment. A 60- to 70-mV positive potential is found in scala media in vivo (31). This endocochlear potential is lost when the temporal bone is isolated from the animal, placing the cochlea in a state where force production by the outer hair cells is reduced to a point where it barely affects sound-evoked responses. All data shown in Fig. 1 were acquired from such "passive" preparations.

To determine the influence of outer hair cell force production on basilar membrane movement, electrical currents (−5 to +5 μA) were injected in scala media and the mechanical response was plotted as a function of current level. The basilar membrane exhibited no measurable response (Fig. 2*A*, *Upper*; mean ± SEM in 15 preparations; note that error bars are too small to be clearly resolved against the mean), not even when currents were increased to ±25 μA. As a control, other regions of the organ of Corti and experimental setup were also examined. No measurable movement when exposed to the current stimulus was shown in Reissner's membrane, the bone surrounding the cochlea, or the electrode tip (Fig. 2*A*, *Lower*).

Because the basilar membrane is attached to both the spiral ligament and the modiolus (schematic drawing in Fig. 2*B*), small vibrations are expected close to either attachment point. We therefore measured current-evoked motion closer to the outer edge of the basilar membrane (Fig. 2*B*, position A) than the standard measurement site (position B), and from the region between the outer and inner hair cells (position C). As seen in the three graphs in Fig. 2*B*, current-evoked motion was absent from all three sites, in direct contrast to the behavior of the Hensen cells (Fig. 2*C*), where substantial current-evoked motion was evident. Negative current displaced Hensen cells toward the scala tympani; they moved in the opposite direction during positive current.

To ascertain that these responses were caused by outer hair cell motility, we applied the commonly used prestin blocker salicylate (32, 33). A 10-min exposure reversibly eliminated current-evoked motion at the Hensen cells (Fig. 2*D*, *Lower Left*; $n = 5$). The basilar membrane, which did not move in response to current, showed no change after salicylate (Fig. 2*D*, *Upper Left*). As a second control, we applied FM1-43, a fluorescent dye that blocks mechanically gated ion channels in hair cells (34). FM1-43 almost abolished current-evoked Hensen cell motion (Fig. 2*D*, *Lower Right*; $n = 3$), although the basilar membrane remained motionless (Fig. 2*D*, *Upper Right*).

A Small Region Under the Outer Hair Cells Moves During Sound Stimulation in Vivo. In the experiments described above, the temporal bone was submerged in tissue culture medium and an opening was created in the bone that surrounds the hearing organ. The extent to which the opening influences the internal sound-evoked motion of the organ of Corti is not known (35), which makes it imperative to verify the above results in a more intact preparation. To this end, we used optical coherence tomography, an interferometric imaging technique that can be used to measure sound-evoked motion in vivo, without creating an artificial opening in the cochlear bone.

The current frequency-domain system (22) allowed simultaneous measurements of basilar membrane and reticular lamina motion, as exemplified in Fig. 3*A*, which shows a vibration measurement superimposed on a structural scan. The colors correspond to displacement magnitude, whereas the structural scan is displayed in grayscale. The resolution in the vertical direction of the structural image was ∼10 μm, which means that delicate features, such as the borders between different cell types within the organ of Corti, were unresolvable. However, the separation between the basilar membrane and the reticular lamina was large, and these structures were easily distinguished. From images such as this one, it was evident that the maximal motion of the basilar membrane occurred in a region 30–50 μm medial to the edge of the organ of Corti (mean of 40 ± 6 μm, $n = 4$, 90 dB SPL stimulus level).

Even at the location of maximum vibration, basilar membrane displacements were smaller than the displacements of the reticular lamina (Fig. 3*B*, *Left*, thick lines; average difference of 3.2 ± 1.1 dB; $P = 0.02$, repeated-measures analysis of variance; $n = 6$). There were no significant phase differences between the basilar membrane and the reticular lamina (Fig. 3*B*, *Right*, thin lines).

The two tuning curves drawn with blue and red solid lines in Fig. 3*C* exemplify data acquired from a single preparation. The shape of the tuning curves was similar, but in three of six cases, basilar membrane vibrations peaked at frequencies higher than the reticular lamina, consistent with the in vitro data described above. We also made attempts to acquire data postmortem, but doing so was difficult, because cells lost reflectivity after the death of the animal. In a limited sample of successful recordings, a

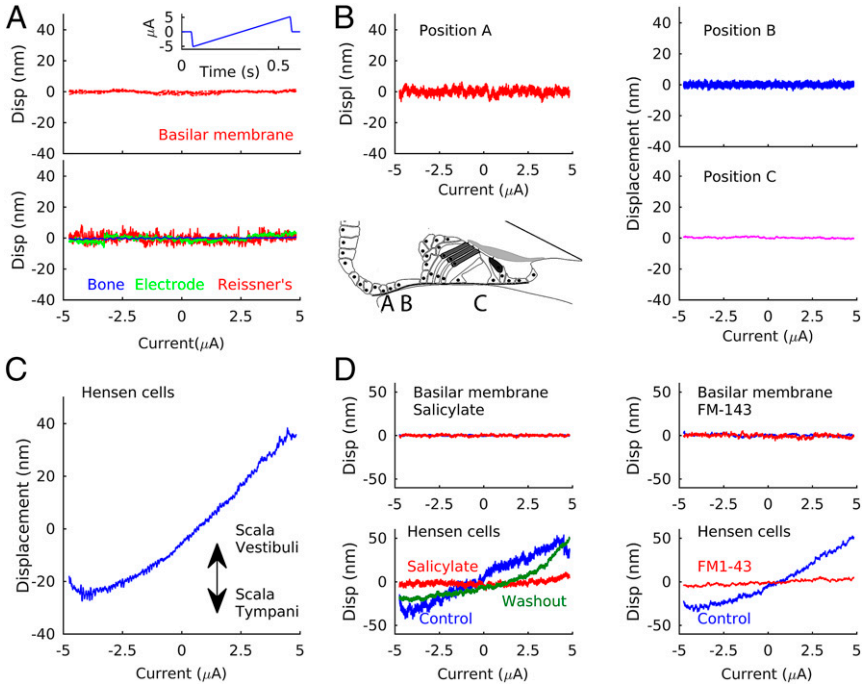

Fig. 2. Minimal basilar membrane movement during electrical stimulation in isolated preparations. (*A*, *Upper*) Current ramps going from −5 to +5 μA (*Inset*) result in no apparent motion at the basilar membrane. (*A*, *Lower*) Lack of electrically evoked motions of bone, the stimulus electrode, and Reissner's membrane. (*B*) Current-evoked displacement (Displ) measured from three separate sites on the basilar membrane (A–C in the schematic drawing). The motion of each site is separately plotted, as indicated by the label on each graph. (*C*) In contrast to the basilar membrane, Hensen cells show large motion during electrical stimulation (−5 to +5 μA). (*D*, *Lower Left*) Current-evoked motion of Hensen cells is reversibly abolished by salicylate (10 mM, stimulus amplitude of −5 to + 5 μA). The basilar membrane is not affected by salicylate (*Upper Left*) or FM1-43 (*Upper Right*), but Hensen cell motion is sharply reduced after application of FM1-43 (*Lower Right*). Disp, displacement.

general decrease of displacement was observed (Fig. 3*C*, blue dashed line illustrates the tuning curve acquired from the reticular lamina in vivo, and black dashed line illustrates the postmortem data from the same structure). There was a tendency for peak vibration to shift toward the inner hair cells, which resulted in increased sound-evoked displacement postmortem for some locations along the reticular lamina. The amplitude, however, did not exceed the one measured in vivo at the original location of peak vibration.

Vibration patterns such as shown in Fig. 3*A* revealed that displacements were slightly larger ∼50 μm down from the reticular lamina, within the body of the organ of Corti, than they were at the reticular lamina (Fig. 3*D*).

As seen in Fig. 3*A*, sound-evoked basilar membrane displacement declined quickly on the sides of the peak, particularly at locations closer to the lateral wall. To characterize this behavior, Fig. 3*E* shows displacement as a function of distance from the location of peak vibration (the vertical line indicates the average position of the lateral edge of the organ of Corti, and the thin red line shows data from the preparation drawn with solid lines in Fig. 3*C*). Displacement decreased exponentially with distance, and the thick red lines are fits of the vibration data to the function:

$$He^{-|y|/\delta},$$

where y is the distance from the peak, H is the peak amplitude, and δ is the length scale of the decay. On the right side of the peak, corresponding to the neural side of the organ of Corti, the length scale was 127 μm (the fit is significant, with $P = 4.5 \times 10^{-8}$ by t test), but it was about fourfold smaller on the abneural side (34 μm; $P = 0.0012$). This exponential decline means that the moving portion of the basilar membrane is relatively small in contrast to the behavior of the basilar membrane at the base of the cochlea (e.g., ref. 36).

The in vitro data shown in Fig. 1*D* were acquired 10–40 μm from the attachment point of the basilar membrane to the lateral wall of the cochlea. In this region, the average basilar membrane displacement was 33 dB below the one measured at the Hensen cells.

In the in vivo experiments, the corresponding points on the basilar membrane showed displacements 27 ± 8 dB below the one measured at the Hensen cells. The more pronounced difference in vitro may be an effect of the opening in the cochlea.

The spatial vibration pattern at the reticular lamina (Fig. 3*F*) was accurately described by linear functions, with slope more than threefold larger on the abneural side (−6.5 nm/μm vs. −2 nm/μm; both $P < 0.005$ by t test; $R^2 = 0.94$ and $R^2 = 0.998$, respectively). A linear change with distance is expected from a structure hinged at one end. The hinge point, or center of vibration, can be found through the linear fits by setting displacement to zero and solving for distance. On the neural side, the hinge point was 250 μm from the peak on average, implying that the reticular lamina vibrated around a point located on the medial side of the inner hair cell, within the fluid of the inner sulcus. Because a constant phase is expected from structures on the same side of the pivot point, data on the phase of vibration along the reticular lamina can be used to corroborate this finding. Phase was found to be constant with distance, both at the basilar membrane and at the reticular lamina (Fig. 3*G*).

On the abneural side of the peak in Fig. 3*F* (negative distance coordinates), displacement fell quickly with distance (slope of −6.5 nm/μm; $R^2 = 0.94$, $P < 0.005$). A decrease in magnitude for the outermost Hensen cells has previously been reported (figure 4B of ref. 18), and our data appear to confirm this finding.

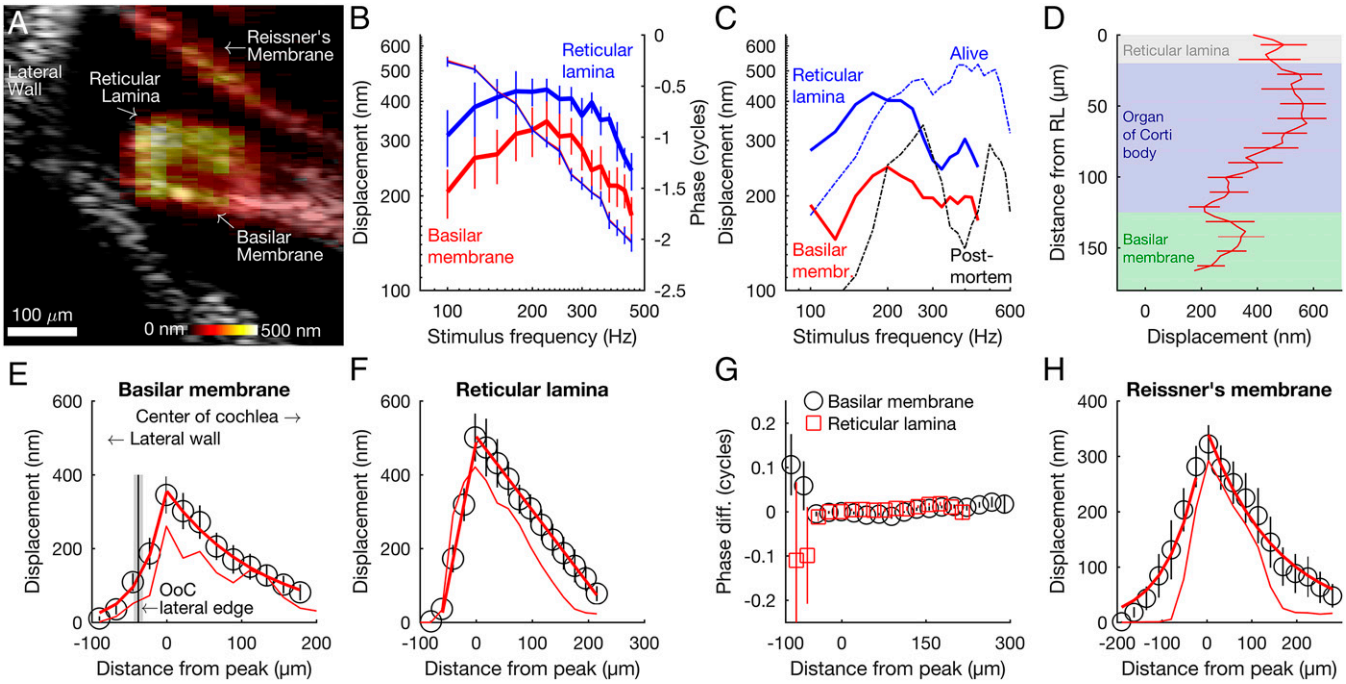

Fig. 3. In vivo motion of the basilar membrane and reticular lamina in closed cochleae. (*A*) Color-coded displacement data were superimposed on a morphological scan (grayscale). The stimulus is a 175-Hz tone at 90 dB SPL. (*B*) Tuning curves at the reticular lamina and at the basilar membrane were similar in shape, but the amplitude at the basilar membrane was smaller. The thick lines show the mean amplitude ± SEM in six preparations, and the thin lines show the corresponding phase values ± SEM. The measurement location is ∼1.5 mm from the helicotrema. (*C*) Tuning curves from the reticular lamina (blue solid line) and basilar membrane (red solid line) in a single preparation. The dashed lines show a reticular lamina tuning curve acquired in vivo (blue dashed line) and postmortem (black dashed line) from a different preparation, where the measurement location was closer to the base of the cochlea than the preparations included in the averaged data in *B*. (*D*) Averaged vibrations of structures in the organ of Corti, from the reticular lamina (RL) toward the basilar membrane ($n = 6$). (*E*) Basilar membrane vibrations peak in an area 30–50 μm medial to the edge of the organ of Corti, but decline rapidly on either side of the peak. The thick red lines are fits to the exponential function given in the main text, and the vertical line and gray zone indicate the average position (±SEM) of the lateral edge of the organ of Corti (OoC) relative to the location of peak vibration. (*F*) Reticular lamina displacement at the best frequency. Thick red lines are fits to the functions $502 - 2 \times$ distance and $475 - 6.5 \times$ distance. (*G*) Phase is invariant with distance from the peak for both the reticular lamina and the basilar membrane. diff., difference. (*H*) Reissner's membrane shows behavior qualitatively similar to the basilar membrane, but the length scale of the exponential decay is different. All vibration data in this figure were acquired at a stimulus level of 90 dB SPL. The thin red lines in *E*, *F*, and *H* show data from the preparation plotted with solid lines in *C*.

Reissner's membrane, which separates scala media from scala vestibuli, showed an exponential relation between displacement and distance from the location of peak vibration (Fig. 3*H*), but the length scale was larger than the one measured at the basilar membrane.

Discussion

Here, we demonstrated that the sound-evoked motion of the basilar membrane is restricted to a region 30–50 μm medial to the edge of the organ of Corti, decreases quickly with radial distance, and is smaller than it is at the Hensen cells (Figs. 1 and 3). The motion of the lateral basilar membrane segment is not influenced by quasistatic outer hair cell force generation (Fig. 2).

Previous work on the low-frequency mechanics of the hearing organ was performed after the creation of an artificial opening in the cochlear bone. The opening may alter sound-evoked vibrations (16, 27, 37) by producing a change in the acoustic impedance of the cochlea. In the in vitro experiments reported here, the preparation is immersed in fluid, which will tend to abolish reflections of acoustic waves from the region of the opening. The result is a loss in effective SPL at frequencies below 300 Hz (27). A similar effect has been observed in in vivo experiments, where there is an opening in the cochlea but no immersion in fluid (16, 37). It seems well established that the opening causes frequency tuning curves to be artificially sharpened, and the present in vivo data are consistent with this possibility, in showing a relatively flat tuning compared with the in vitro preparations. The effect of the opening on the fast acoustic waves present in the cochlea is controversial (cf. ref. 37 vs. ref. 38), as are the possible effects of the opening on the internal motion of the organ of Corti (35). Opening of the cochlea may also impart substantial trauma, the effect of which is difficult to determine because common methods for assessing the physiological status of the cochlea do not work well at low frequencies. The uncertainties about the effects of the opening make it important to perform experiments in more intact preparations, but the techniques for performing such measurements only recently became available (22, 23).

Our data show that the best frequency of the basilar membrane often is higher than the one measured at the Hensen cells. Differences in the best frequency among different structures have been found at the base of the cochlea (39), where the basilar membrane was tuned to a frequency lower than the reticular lamina, underscoring the difference between high- and low-frequency cochlear regions.

A significant new finding reported here is the nearly exponential decay of basilar membrane vibration with radial distance (Fig. 3). Some previous studies, most of which were performed after seeding the basilar membrane with reflective beads through small tears in Reissner's membrane, found that the basilar membrane and Hensen cells had similar amplitudes of sound-evoked motion (19–21, 40). Other studies, using no artificial reflectors, found basilar membrane movements to be 25–60 dB smaller than the Hensen cell magnitude (15, 17, 18). Apart from a possible effect from mixing endolymph and perilymph, an explanation for these

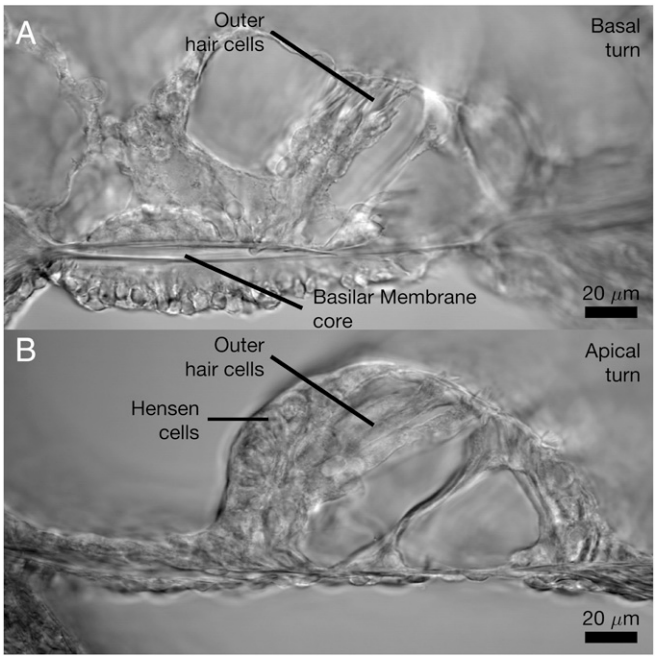

Fig. 4. Morphological differences between the basal and apical turns may contribute to the sound-evoked motion of the basilar membrane. (*A*) In the basal cochlear turn, the basilar membrane has a dense core surrounded on both sides by layers of cells. (*B*) In the apical turn, the dense core is replaced by a thin layer of tissue that runs through the width of the basilar membrane.

differences may be that the strong reflection from the bead allows vibration measurements from sites close to the organ of Corti, where the present in vivo data show somewhat smaller differences between Hensen cell and basilar membrane vibrations. The long wavelength and short coherence length of the light source, however, lead to a clear improvement in accessibility when optical coherence tomography is used.

The structure of the basilar membrane is expected to shape its response to sound stimulation. At the base, a thick layer of fibers form a dense core (Fig. 4*A*) with high bending stiffness (36). The dense core means that a beam model captures the essential aspects of basilar membrane mechanics, predicting a radial deformation profile with a broad peak, in agreement with measurements from the base of the cochlea. Toward the apex, the basilar membrane is wider, its fibers become thinner, and the core structure is absent, which reduces stiffness (Fig. 4*B*). Our finding of a radial deformation profile with a sharp peak and exponential decay shows that the apical basilar membrane cannot be described by simple beam models.

Some of the present findings are consistent with the ratchet theory of low-frequency hearing (14). The ratchet mechanism implies that outer hair cell force generation minimizes fluid displacement, which could be consistent with the small motion of the lateral segment of the basilar membrane. The higher best frequency of the basilar membrane would also be consistent with this theory. However, additional experiments are required to prove this theory conclusively. Nevertheless, the present experiments show an unexpected response pattern at the basilar membrane that is relevant for understanding how speech-frequency sound is detected by the hearing organ.

Methods

In Vitro Preparation. Using procedures approved by the Linköping University Ethics Committee (permit N32/13), young guinea pigs (200–400 g) were anesthetized and euthanized. The temporal bones were removed and attached to a custom-made holder allowing direct sound stimulation of the tympanic membrane, and the bulla was opened to expose the middle ear. The preparation was submerged in oxygenated tissue culture medium (minimum essential medium; Invitrogen), reducing the effective sound pressure by ∼25 dB. An ∼0.35-mm^2 triangular opening was made in the apex 120° from the helicotrema. The opening covered ∼15% of the apex, and it was similar to the one used in a previous study (20) and slightly larger than the one used to obtain in vivo data in a previously published study (37). A beveled borosilicate glass electrode was placed in scala media, penetrating the otherwise intact Reissner's membrane. This electrode was used to monitor the sound-evoked cochlear microphonic potential, using a Dagan instruments IX1 amplifier with a head-stage having a magnification of 10×. Data collection was aborted if these potentials, measured throughout the experiment, underwent sudden changes. An optically isolated constant current stimulator (A395; WPI) was used for injecting currents through the electrode utilized for measuring cochlear microphonic potentials; the amplitude of the current-evoked motions was used as a secondary quality indicator. The ground electrode was placed in the fluid surrounding the preparation. Scala tympani were continuously perfused with oxygenated medium (∼0.6 mL·h^{-1}), beginning within 10 min of decapitation. The perfusion system was used to deliver drugs to the hair cells. All experiments were carried out at room temperature (21–24 °C).

Interferometry and Confocal Imaging. A custom-built displacement-sensitive interferometer (noise floor <0.1 nm/$\sqrt{\text{Hz}}$ at frequencies above 10 Hz) with a lens with a magnification of 25× was used for measuring acoustically and electrically evoked motion of the organ of Corti. The system, which is described in detail elsewhere (26), allows measurements without the use of artificial reflectors. The preparation was oriented with the basilar membrane perpendicular to the optical (transverse) axis. The orientation was confirmed by imaging using a Zeiss LSM Pascal confocal microscope integrated with the interferometer. Both systems shared the same objective lens, and careful alignment ensured that the difference in focal planes was less than 1 μm. Confocal images were used for 3D reconstructions, utilizing Imaris software (Bitplane AG). Displacement data were averaged 10 times. If the signal was unstable, the measurement was rejected. A linear ramp going from +5 μA to −5 μA (or the inverse) over the course of 500 ms was used for current injection (Fig. 2*A*, *Inset*). Each current ramp was preceded by 50 ms of data acquisition at zero current.

Sound Stimulation. The dissection described above leaves the tympanic membrane and middle ear ossicles intact, so sound stimulation was applied through a loudspeaker positioned in the ear canal. The loudspeaker was driven by a function generator (model 33120A; Agilent Technologies) and a digital attenuator. Vibration was measured at sound pressures ranging from 44 to 119 dB SPL (these sound pressures are the measured levels from the loudspeaker; all sound pressure values given in the part of the main text describing in vitro data were corrected for a 25-dB attenuation caused by the immersion of the preparation in tissue culture medium).

Data Acquisition and Signal Processing. All data were collected by custom Labview software that controlled a 12-bit board sampling the amplified carrier signal of the interferometer. Microphonic potentials were sampled by a 16-bit board. All data processing was performed off-line using custom MATLAB (MathWorks) scripts.

In Vivo Experiments. In vivo experiments, and the immunolabeling described below, were carried out using procedures approved by the Institutional Review Board at Oregon Health & Science University. In brief, young guinea pigs were anesthetized with a combination of ketamine (40 mg/kg of body weight) and xylazine (10 mg/kg of body weight). Supplemental doses were given hourly. Throughout the surgical procedures and mechanical measurements, animal temperature was maintained at 38 °C, using a feedback-controlled heating pad wrapped around the animal. The auditory bulla was exposed using standard surgical techniques (41); however, in contrast to previous studies, no artificial opening was created in the cochlea. Instead, a small mirror assembly was mounted on its apex. The infrared light beam of the optical coherence tomography system was aimed at the mirror, which reflected the light through the bone onto the cells of the organ of Corti. This arrangement made it possible to measure sound-evoked vibrations in an undisturbed cochlea in the direction perpendicular to the basilar membrane. Such measurement would otherwise require extensive dissection, which easily causes severe trauma to the delicate sensory cells in the inner ear.

Optical Coherence Tomography. Vibration of the organ of Corti was measured with a phase-sensitive optical coherence tomography system (22). In this device, the 840-nm light generated by a broad-band superluminescent diode

passes through the measurement system to illuminate the cells of the organ of Corti, reaching them through the intact cochlear bone. The back-reflected light is combined with a reference beam of light to form a spectral interference signal that is detected by a sensitive optical spectrometer. This technique allows the displacement of each reflecting structure to be calculated with a sensitivity of ~50:00 picometers, using custom Labview data acquisition software. The spatial resolution of the system is ~10 μm.

Histology. Albino Dunkin–Hartley guinea pigs were euthanized and perfused intracardially with 0.1 M PBS, followed by 4% (vol/vol) paraformaldehyde. The cochleae were decalcified in 10% EDTA for 7–10 d and embedded in 4% (vol/vol) agarose, and 120-μm sections were cut on a Leica VT1000 vibratome. The sections were visualized on an Olympus Fluoview FV1000 confocal laser microscope system using the transmission detector and a 40× lens with a 1.3 numerical aperture.

ACKNOWLEDGMENTS. We thank Gemaine Stark and Sarah Foster for the harvest and vibratome sectioning of guinea pig cochleae. This study was supported by Swedish Research Council Grant K2014-63X-14061-14-5 (to A.F.); the Torsten Söderberg Foundation (A.F.); the Stiftelsen Tysta Skolan (A.F.); the Strategic Research Area for Systems Neuroscience (A.F.); and NIH National Institute on Deafness and other Communication Disorders Grants DC 00141 and 000105 (to A.L.N.), Grant DC 005983 (to Peter Barr-Gillespie), Grant NS 061800 (to Sue Aicher), and Grant R01 DC 010399 (to A.L.N, R.K.W, and S.L.J.).

1. von Békésy G (1960) *Experiments in Hearing* (McGraw–Hill, New York).
2. Robles L, Ruggero MA (2001) Mechanics of the mammalian cochlea. *Physiol Rev* 81(3): 1305–1352.
3. Ren T (2002) Longitudinal pattern of basilar membrane vibration in the sensitive cochlea. *Proc Natl Acad Sci USA* 99(26):17101–17106.
4. de La Rochefoucauld O, Olson ES (2007) The role of organ of Corti mass in passive cochlear tuning. *Biophys J* 93(10):3434–3450.
5. Zheng J, et al. (2000) Prestin is the motor protein of cochlear outer hair cells. *Nature* 405(6783):149–155.
6. Ashmore J (2008) Cochlear outer hair cell motility. *Physiol Rev* 88(1):173–210.
7. Martin P, Hudspeth AJ (1999) Active hair-bundle movements can amplify a hair cell's response to oscillatory mechanical stimuli. *Proc Natl Acad Sci USA* 96(25):14306–14311.
8. Martin P, Hudspeth AJ (2001) Compressive nonlinearity in the hair bundle's active response to mechanical stimulation. *Proc Natl Acad Sci USA* 98(25):14386–14391.
9. Kennedy HJ, Crawford AC, Fettiplace R (2005) Force generation by mammalian hair bundles supports a role in cochlear amplification. *Nature* 433(7028):880–883.
10. Fisher JA, Nin F, Reichenbach T, Uthaiah RC, Hudspeth AJ (2012) The spatial pattern of cochlear amplification. *Neuron* 76(5):989–997.
11. Reichenbach T, Hudspeth AJ (2010a) Dual contribution to amplification in the mammalian inner ear. *Phys Rev Lett* 105(11):118102.
12. Ren T, He W, Li Y, Grosh K, Fridberger A (2014) Light-induced vibration in the hearing organ. *Sci Rep* 4:5941.
13. Nuttall AL, Dolan DF (1996) Steady-state sinusoidal velocity responses of the basilar membrane in guinea pig. *J Acoust Soc Am* 99(3):1556–1565.
14. Reichenbach T, Hudspeth AJ (2010b) A ratchet mechanism for amplification in low-frequency mammalian hearing. *Proc Natl Acad Sci USA* 107(11):4973–4978.
15. Khanna SM, Flock A, Ulfendahl M (1989) Comparison of the tuning of outer hair cells and the basilar membrane in the isolated cochlea. *Acta Otolaryngol Suppl* 467: 151–156.
16. Cooper NP, Rhode WS (1996) Fast traveling waves, slow traveling waves, and their interactions in experimental studies of cochlear mechanics. *Auditory Neuroscience* 2:289–299.
17. Hao LF, Khanna SM (2000) Vibrations of the guinea pig organ of Corti in the apical turn. *Hear Res* 148(1-2):47–62.
18. Khanna SM, Hao LF (2000) Amplification in the apical turn of the cochlea with negative feedback. *Hear Res* 149(1-2):55–76.
19. Cooper NP, Rhode WS (1995) Nonlinear mechanics at the apex of the guinea-pig cochlea. *Hear Res* 82(2):225–243.
20. Hemmert W, Zenner H, Gummer AW (2000) Characteristics of the travelling wave in the low-frequency region of a temporal-bone preparation of the guinea-pig cochlea. *Hear Res* 142(1-2):184–202.
21. Hemmert W, Zenner HP, Gummer AW (2000) Three-dimensional motion of the organ of Corti. *Biophys J* 78(5):2285–2297.
22. Ramamoorthy S, et al. (2016) Minimally invasive surgical method to detect sound processing in the cochlear apex by optical coherence tomography. *J Biomed Opt* 21(2):25003.
23. Lee HY, et al. (2015) Noninvasive in vivo imaging reveals differences between tectorial membrane and basilar membrane traveling waves in the mouse cochlea. *Proc Natl Acad Sci USA* 112(10):3128–3133.
24. Fridberger A, Tomo I, Ulfendahl M, Boutet de Monvel J (2006) Imaging hair cell transduction at the speed of sound: Dynamic behavior of mammalian stereocilia. *Proc Natl Acad Sci USA* 103(6):1918–1923.
25. Hakizimana P, Brownell WE, Jacob S, Fridberger A (2012) Sound-induced length changes in outer hair cell stereocilia. *Nat Commun* 3:1094.
26. Jacob S, Johansson C, Ulfendahl M, Fridberger A (2009) A digital heterodyne laser interferometer for studying cochlear mechanics. *J Neurosci Methods* 179(2):271–277.
27. Ulfendahl M, et al. (1996) Mechanical response characteristics of the hearing organ in the low-frequency regions of the cochlea. *J Neurophysiol* 76(6):3850–3862.
28. Kelly JP (1989) Cellular organization of the Guinea pig's cochlea. *Acta Otolaryngol Suppl* 467:97–112.
29. van der Heijden M, Joris PX (2003) Cochlear phase and amplitude retrieved from the auditory nerve at arbitrary frequencies. *J Neurosci* 23(27):9194–9198.
30. Ruggero MA, Rich NC, Recio A, Narayan SS, Robles L (1997) Basilar-membrane responses to tones at the base of the chinchilla cochlea. *J Acoust Soc Am* 101(4): 2151–2163.
31. Conlee JW, Bennett ML (1993) Turn-specific differences in the endocochlear potential between albino and pigmented guinea pigs. *Hear Res* 65(1-2):141–150.
32. Shehata WE, Brownell WE, Dieler R (1991) Effects of salicylate on shape, electromotility and membrane characteristics of isolated outer hair cells from guinea pig cochlea. *Acta Otolaryngol* 111(4):707–718.
33. Hakizimana P, Fridberger A (2015) Effects of salicylate on sound-evoked outer hair cell stereocilia deflections. *Pflugers Arch* 467(9):2021–2029.
34. Gale JE, Marcotti W, Kennedy HJ, Kros CJ, Richardson GP (2001) FM1-43 dye behaves as a permeant blocker of the hair-cell mechanotransducer channel. *J Neurosci* 21(18): 7013–7025.
35. de Boer E (1990) Wave-propagation modes and boundary conditions for the Ulfendahl-Flock-Khanna preparation. *The Mechanics and Biophysics of Hearing*, eds Dallos P, Geisler CD, Matthews JW, Ruggero MA, Steele C (Springer, Berlin), pp 333–339.
36. Homer M, Champneys A, Hunt G, Cooper N (2004) Mathematical modeling of the radial profile of basilar membrane vibrations in the inner ear. *J Acoust Soc Am* 116(2): 1025–1034.
37. Dong W, Cooper NP (2006) An experimental study into the acousto-mechanical effects of invading the cochlea. *J R Soc Interface* 3(9):561–571.
38. Zinn C, Maier H, Zenner H, Gummer AW (2000) Evidence for active, nonlinear, negative feedback in the vibration response of the apical region of the in-vivo guinea-pig cochlea. *Hear Res* 142(1-2):159–183.
39. Ramamoorthy S, et al. (2014) Filtering of acoustic signals within the hearing organ. *J Neurosci* 34(27):9051–9058.
40. Gummer AW, Hemmert W, Zenner H-P (1996) Resonant tectorial membrane motion in the inner ear: Its crucial role in frequency tuning. *Proc Natl Acad Sci USA* 93(16): 8727–8732.
41. Zheng J, et al. (2011) Persistence of past stimulations: Storing sounds within the inner ear. *Biophys J* 100(7):1627–1634.